Applied Clay Science 277 (2025) 107969

Contents lists available at ScienceDirect

Applied Clay Science

journal homepage: www.elsevier.com/locate/clay

Research Paper

Effect of mechanical activation on the structural, morphological and textural properties of synthetic high-charge micas☆

Aníbal López-Marín [a], Fernando Aguado [b,c], Rosa Martín-Rodríguez [a,b,*], Ana C. Perdigón [a,b,*]

[a] QUIPRE Department, Universidad de Cantabria, Avda. de Los Castros, 46, 39005 Santander, Spain
[b] Nanomedicine Group, IDIVAL, Avda. Cardenal Herrera Oria s/n, 39011 Santander, Spain
[c] CITIMAC Department, Universidad de Cantabria, Avda. de Los Castros, 48, 39005 Santander, Spain

ARTICLE INFO

Keywords:
High-charge micas
Ball milling
Mechanical activation
Particle size reduction

ABSTRACT

Dry grinding is an effective method for mechanically activating clay minerals to enhance their efficiency in various material applications. This is achieved by increasing the number of exposed active sites and the overall surface area through particle size reduction. Nevertheless, this method frequently results in a reduction of crystallinity or alterations in the structure of the clay material. In this context, trioctahedral clays with a high aluminum content exhibit greater structural resistance to degradation. Thus, this work aimed to employ dry grinding as an effective top-down nano-sintering method to obtain nano-clays from the high-charge mica family. High-charge micas are a group of trioctahedral synthetic micas with aluminum in the tetrahedral layer, widely studied because of their interesting adsorption properties. The novelty of this work laid in demonstrating that dry grinding can effectively reduce the particle size of high-charge micas to the nanoscale while preserving their structural integrity, representing a significant advancement in the controlled mechanical activation of trioctahedral clays without inducing amorphization. To reduce the risk of amorphization, gentle milling conditions were applied using a planetary ball mill. After 15 min of grinding at 500 rpm, a substantial reduction in particle size from microns to the nanoscale was obtained, while preserving the long and short-range order of the material. Moreover, despite prolonged grinding, an increase in external surface area was still evident, while the characteristic structural properties of micas remained intact. Montmorillonite, a natural clay mineral, was used as a reference for comparing the structural and textural properties under equivalent grinding conditions.

1. Introduction

Mechanical activation (MCA) is a common method used to enhance the efficiency of clay minerals in various material and civil engineering applications, such as contaminant adsorption -including drugs-, water remediation, and agricultural fertilizers, among others (Nasser and Mingelgrin, 2012; Baláž et al., 2013; Said et al., 2018; Morantes et al., 2020). Clay minerals are widely used because they are abundant in nature, cheap, environmentally friendly, and non-hazardous materials. In particular, clay minerals were proposed to be part of the engineering barrier as adsorbents to ensure the long-term safety of radioactive waste management (Kim et al., 2025). Mechanical activation of the material was expected to cause an increment in the number of active sites exposed after grinding, modification of the exchange cation capacity, creation of new meso- or microporosity, increment of the specific surface area, and reduction of the particle size (Christidis et al., 2005; Trujillano et al., 2010; Valera-Zaragoza et al., 2021). All those modifications are carried out to enhance the properties of the material for each specific application. In particular, the adsorption and physicochemical properties of clays can be enhanced by decreasing their dimensions to the nanoscale. Increasing the specific surface area by nano-sintering using top-down approaches can also modify the mechanisms involved in the adsorption phenomena. Among the different top-down approaches, the dry grinding method showed significant results in reducing particle size. However, this process was often accompanied by a partial loss of crystallinity or structural changes in various clays, such as kaolin (Elhadj and Perrin, 2021; Mañosa et al., 2023), kaolinite (Ji and Zhang, 2021; Machida et al., 2023), talc (Dellisanti et al., 2011; Kim et al., 2019), pyrophyllite (Sanchez-Soto and Perez-Rodriguez, 1989; Zhang et al., 2015) and montmorillonite (Hrachová et al., 2007; Vdovic et al., 2010;

☆ This article is part of a Special issue entitled: 'Clay Conf. Hannover 2024' published in Applied Clay Science.

* Corresponding authors at: QUIPRE Department, Universidad de Cantabria, Avda. de Los Castros, 46, 39005 Santander, Spain.
E-mail addresses: rosa.martin@unican.es (R. Martín-Rodríguez), perdigonac@unican.es (A.C. Perdigón).

https://doi.org/10.1016/j.clay.2025.107969
Received 16 April 2025; Received in revised form 19 July 2025; Accepted 11 August 2025
Available online 19 August 2025

Maleki and Karimi-Jashni, 2017), among others.

Different milling media configurations are used for dry grinding, in particular by ball milling, planetary ball milling or vibratory disc mill. However, the effectiveness of dry grinding strongly depends on the conditions of the milling process, as milling media, angular speed and time grinding. Additionally, in the ball milling technique it is crucial to optimize the ball-to-powder ratio (BPR) and select an appropriate diameter of the balls (Tole et al., 2019). Milling media involves the use of vessels and balls made by the same or different materials with similar hardness, in the range of 4.5–9 of Mohs scale. Frequent milling media materials include stainless steel, carbides, porcelain, agate, aluminum oxide, corundum, and zirconia (Baláž et al., 2013).

The diameter of balls also plays an important role in the grinding behavior of clay powders; as the mass or diameter of the ball increases, the number of higher collision impacts between balls and powder occurs, permitting reducing the particle size of the starting material in less grinding time. For instance, intensive grinding of talc, a 2:1 layered clay mineral, using different ball sizes was reported, suggesting that smaller diameter of balls media causes less structural damage to characteristic (00*l*) basal reflection of talc mineral as time grinding increases (Kim et al., 2019). However, larger diameters of balls in dry grinding treatment performed a significant increase in specific surface area of the original clay due the effectiveness of high-impact collisions and, consequently, a formation of new accessible actives sites.

Different results under similar grinding conditions, mainly in the morphology and structure of clays, were obtained according to the clay type, layer charge distribution, and the composition of the octahedral sheet. For instance, structural transformation of kaolinite, a 1:1 type clay mineral, was caused after 2 h of mechanical milling, by the breaking of the structural hydroxyl groups and substitution by water molecules coordinated and adsorbed on the surface (Frost et al., 2001). Also, after 10 h of intensive ball milling, kaolinite reduced its crystallinity and increased the specific surface area, probably due to the formation of a new silicate phase. Pálková et al. (2021) reported the influence of the octahedral sheets composition on the structural changes of a set of trioctahedral and dioctahedral smectites under short duration dry grinding. Apparently, trioctahedral nature had a stabilization effect, as the trioctahedral clays were less affected than the dioctahedral ones under similar grinding conditions. In addition, a second parameter became important in the resistance to amorphization: the aluminum content in the tetrahedral layer, since higher AlO_4 content implies better structural stability (Pálková et al., 2021). Despite these differences, a similar pattern of behavior occurred in all cases: an alteration of the structural hydroxyl groups, followed by the disruption of the tetrahedral and octahedral layers, and finally, the formation of a less crystalline phase and amorphization. These changes were generally accompanied by a reduction in particle size, followed by a decrease in surface area, typically attributed to agglomeration phenomena (Tole et al., 2019).

Comparative studies were mainly conducted on a selection of dioctahedral and trioctahedral smectites, which are 2:1 low-charge aluminosilicates. According to the literature, few studies were focused on clays with a higher aluminum content. In this regard, Osuna et al. (2023) presented the effects of mechanical activation on the family known as high-charge micas, a group of synthetic aluminosilicates rich in tetrahedral aluminum, after grinding in a vibratory disc mill. Changes in the texture and structure of clays, including the loss of long-range order, the formation of new crystalline phases, and the creation of mesoporosity and microporosity were reported. However, an increase in particle size and polydispersity was exhibited with mechanical treatment up to 150 s, which was associated with particle agglomeration.

The aim of this research was to employ dry grinding as an effective top-down nano-sintering method to obtain mechanically activated nanoclays from the high-charge mica family. Long treatment times and mild milling conditions in a planetary ball mill were chosen to prevent amorphization as much as possible. Decreasing the particle size will increase the number of exposed active sites, improving the effectiveness of the clayey material in certain industrial applications, such as adsorbents for soil decontamination, rare earths elements recovery mechanisms (Iannicelli-Zubiani et al., 2015; Xiao et al., 2016; Alshameri et al., 2019; Fang et al., 2021) or as acidic materials in catalysis, for instance. In particular, high-charge micas were investigated as a serious alternative to smectites for use as engineered barriers in deep geological repositories, aiming to permanently retain high-level radioactive waste through the formation of new crystalline phases under hydrothermal conditions. In this retention mechanism, the active sites were associated with aluminum located in the tetrahedral sheet of the aluminosilicate structure. Reducing the particle size to the nanoscale increases the number of aluminum ions exposed on the surface, which may lead to enhanced reactivity in the nanoclays.

Hence, Na-*n*-micas ($n = 2, 4$) synthesized by NaCl melt method were post-treated by dry grinding in a planetary ball milling at different grinding conditions. The samples, which are trioctahedral and have a high aluminum content, were selected based on the parameters reported to offer better resistance to amorphization. The optimum grinding conditions to obtain activated clays with a nanoscale particle size while preserving their structure were determined. The structural and textural properties were also compared with those of montmorillonite, a natural clay source, under similar grinding conditions. Montmorillonite is a dioctahedral smectite in which the layer charge arises from the isomorphic substitution of aluminum mainly by iron and magnesium in the octahedral sheet. This clay mineral was selected due to its extensive investigation under milling conditions (Hrachová et al., 2007; Bekri-Abbes and Srasra, 2016).

2. Experimental

2.1. Materials

For the synthesis of Na-*n*-micas ($n = 2, 4$), with the structural formula $Na_nSi_{(8-n)}Al_nMg_6O_{20}F_4$, starting reactants employed were fumed SiO_2 from Sigma-Aldrich (CAS no. 112945–52-5, 99.8 % purity), $Al(OH)_3$ from Riedel-de Häen (CAS no. 21645–51-2, 99 % purity), MgF_2 from Sigma (CAS no. 7783-40-6, 99.9 % purity) and NaCl from Merck (CAS no. 7647-14-5, 99.5 % purity). For comparison of physicochemical properties with other clays, montmorillonite SWy-2 (County of Crook, Wyoming, US) with the chemical formula $(Ca_{0.12}Na_{0.32}K_{0.05})[Al^{01}_{3.}Fe^{3+}_{0.41}Mn_{0.01}Mg_{0.54}Ti_{0.02}][Si_{7.98}Al_{0.02}]O_{20}(OH)_4$, was used as a natural clay source.

2.2. Synthesis Method

All Na-*n*-mica samples were prepared following the NaCl melt procedure (Alba et al., 2006). Near-stoichiometric powder mixtures with the molar compositions (8-*n*) SiO_2, (*n*) $Al(OH)_3$, 6 MgF_2, and (2*n*) NaCl were used for the synthesis of Na-*n*-micas ($n = 2, 4$). All solid reactants were vigorously ground in an agate mortar and subsequently heated in Pt crucibles at 900 °C for 15 h. After cooling, the solid mixtures were washed with deionized water, centrifugated and dried at 50 °C for 48 h.

2.3. Ball milling process

Dry grinding of clay minerals was carried out in a planetary ball mill (FM-100, Retsch), consisting of one zirconia container of 50 mL and zirconia balls with a diameter of 5 mm as milling media. In order to assess the effect on the structure of natural clays and synthetic micas, a BPR of 20:1 was employed with a milling speed of 500 rpm. The milling process was studied at different grinding times (5, 15, 30, 60, and 120 min). All powder samples (500 mg) of synthesized Na-*n*-micas and natural montmorillonite SWy-2 (MMT) were ground at the same milling conditions. Unmilled and milled samples were denotated according to clay source and dry grinding time treatment (DG). Hence, powdered samples were identified as clay-DGX, whereas X represents the grinding

time in minutes.

2.4. Characterization

The X-ray powder diffraction (XRD) pattern of samples were obtained with Rigaku Miniflex instrument, and were recorded by Cu Kα radiation (λ = 1.5418 Å) at 40 kV and 15 mA. Diffractograms were obtained, from 2 to 70° 2θ at a scanning speed of 5°/min with a scan step of 0.03°, at ambient conditions. Configuration set up included a 2.5° soller slit on the incident beam and a 0.625° divergent slit (DS), with incident height slit (IHS) of 10 mm. For sample preparation, each clay was previously dried at 50 °C in air atmosphere and stored, before XRD pattern analysis. Interbasal spacing *d* of clays were determined according Bragg's Law where $\lambda = 2 \cdot d \cdot \sin(\theta)$.

Termogravimetric analysis (TG) was carried out by thermogravimetric analyzer Perkin Elmer TGA 4000 instrument. The samples were placed into a zirconia crucible in a synthetic air atmosphere during the heating period, from 20 to 900 °C by a constant rate of 10 °C/min.

Changes in morphology, and particle size of samples before and after dry grinding were analyzed by transmission electron microscopy (TEM) and scanning electron microscopy (SEM). TEM was performed in a JEOL JEM 1011 microscope. For TEM measurements the powder was suspended in deionized water at 1:2000 solid/liquid ratio and 20 μL of suspension was deposited on a carbon-coated copper grid. SEM images

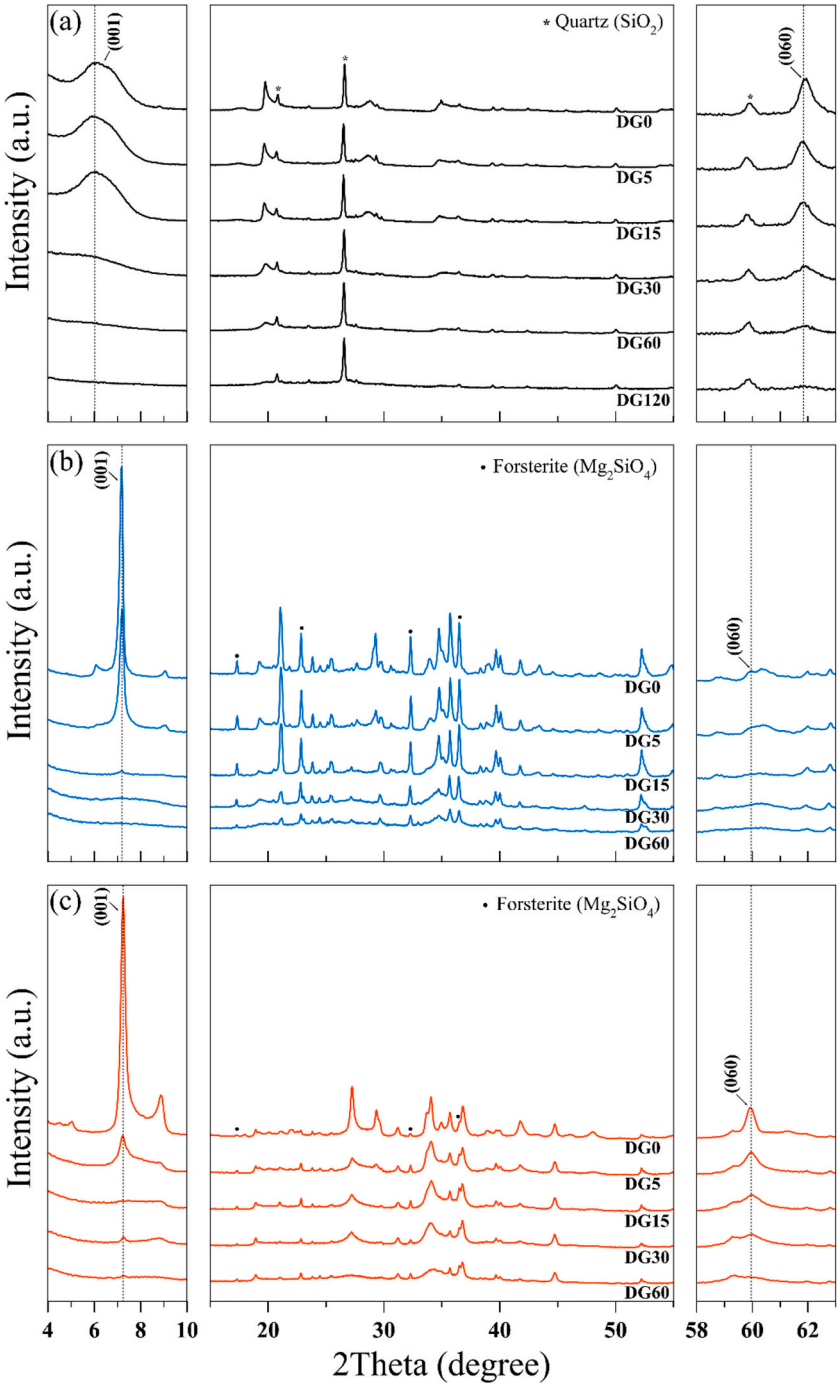

Fig. 1. XRD patterns of MMT (a) Na-2-mica (b) and Na-4-mica (c) unmilled and ground samples at different grinding times. Secondary phases are marked in the diagrams.

were acquired in a Phenom Pharos G2 Desktop Field Emission Gun-Scanning Electron Microscopy (FEG-SEM) and recorded at 20 kV.

The specific surface area and porosity analysis were assessed using N_2 adsorption-desorption isotherms with a Micromeritics ASAP 2420 surface analyzer and porosimetry system. Prior to analysis, the samples were outgassed at 393 K overnight. The specific surface area (S_{BET}) was calculated using the Brunauer–Emmett–Teller (BET) method, while the micropore and mesopore volumes were obtained from the t-plot and Density Functional Theory (DFT) methods, respectively.

Fourier Transform Infrared (FTIR) spectra of the samples were obtained in the range of 4000 to 400 cm^{-1} by a FTIR Jasco 4200 Spectrometer instrument, with 200 scans per sample and resolution of 1 cm^{-1}. FTIR transmission spectra were collected using the KBr pellets technique, in order of 2 mg of powder sample per 198 mg of KBr.

3. Results and discussion

3.1. Effect of dry grinding on clay structure

The long-range order of the samples was analyzed using the XRD technique. Fig. 1 (a) presents the XRD patterns of the montmorillonite sample before and after grinding at different times up to 120 min. For the initial montmorillonite sample, the XRD pattern had an intense basal (001) reflection situated at $2\theta = 6.03^\circ$, with a basal spacing of d_{001}-value = 14.7 Å, indicating the predominant presence of hydrated Ca^{2+} in the interlayer.

Asymmetric (*hk*0) general reflections were also detected in the montmorillonite diffractogram, which are directly related to the bidimensional structure of the clay. Additionally, the (060) reflection provides information on octahedral occupancy, allowing for the distinction between trioctahedral and dioctahedral smectites. The d_{060}-value calculated was 1.49 Å as expected for a dioctahedral clay. A secondary crystalline phase, quartz, was identified and marked with an asterisk in the pattern.

The XRD patterns of the ground samples were analyzed to assess how grinding influences their long-range order. The evolution of both types of reflections substantially differed with the time of grinding. Basal and general reflections remained almost unperturbed with the first 15 min of grinding. As grinding time increased, the basal reflections of montmorillonite samples began to decrease significantly and completely disappear with 30 min of grinding, indicating the delamination of the clay. Different arguments were proposed to explain the loss of basal reflections after treatment. Xia et al. (2010) reported a shift of the (001) reflection to lower angles and a consequent increase in the basal spacing value when purified montmorillonite was ground in a planetary ball mill. The authors attributed this behavior to the peeling off between the layers of montmorillonite. However, in the present work, no displacement of the basal reflections was detected, and the delamination resulted from direct damage rather than exfoliation, according to other studies (Valera-Zaragoza et al., 2021). The absence of the (001) reflection suggests that the stacking of the layers became disordered and eventually disappears. Structural reflections (*hk*0) are less affected by grinding. From 15 to 60 min, structural reflections underwent a progressive decrease in intensity and broadening, yet remaining visible in the pattern, confirming that the bidimensional structure of the clay mineral was damaged but still preserved. However, after 120 min of treatment, structural changes in the sample became evident in the diagram, and only the crystalline quartz phase remained. Several authors suggested the possibility that quartz, which is present in the original sample, acts as an additional grinding body, accelerating the amorphization of montmorillonite (Maleki and Karimi-Jashni, 2017). The diffraction pattern of the ground sample after 120 min exhibited a broad hump in the 2θ range of approximately 15–35°, typical of Si-based amorphous phases.

XRD patterns of Na-*n*-mica (n = 2 and 4) unmilled and ground samples at different grinding times up to 60 min are included in Fig. 1(b) and (c). High-charge micas are synthetic trioctahedral clays in which all octahedral sites are fully occupied by Mg^{2+} ions. The layer charge, ranging from 2 to 4 negative charges per unit cell, is generated by the isomorphic substitution of Si^{4+} by Al^{3+} in the tetrahedral sheet. Unlike natural micas, this charge is compensated by hydrated Na^+ in the interlayer space of the aluminosilicate. XRD diagrams of both raw samples consisted of a set of reflections corresponding to the principal mica phase type and a second group of reflections associated with impurities, mainly forsterite. This phase was described in the literature as a secondary product of the synthesis process (Alba et al., 2006). Unmilled Na-2-mica and Na-4-mica displayed well-defined (00*l*) basal reflections with a high-intensity reflection at $2\theta = 7.2^\circ$, which can be attributed to Na^+ ions with a monolayer of water in the mica interlayer, corresponding to an interbasal spacing of d_{001}-value = 12.2 Å. Both micas also exhibited a lower-intensity (001) reflection at $2\theta \approx 9^\circ$, indicating the presence of a partially dehydrated mica phase. A significant-intensity (060) reflection at $2\theta = 60^\circ$ was also detected in both micas. The calculated d_{060}-value was 1.54 Å, consistent with the trioctahedral character of the samples.

Similar to other clays, the damage caused by grinding varied depending on the dimension, being greater in the z-axis than in the a-b plane (Bekri-Abbes and Srasra, 2016). Basal plane reflections became progressively broader and decreased in intensity during the first 5 min of activation, rapidly disappearing after 15 min of intensive grinding in both Na-*n*-mica samples. However, the position of the (001) reflection was maintained, indicating the same delamination mechanism as in montmorillonite. Despite the stacking of the layers being lost at early times, 15 min, structural reflections were still present during milling treatment up to 60 min and can be attributed to the prevalence of the long-range arrangement of clay layers. Structural reflections in both micas progressively decreased in intensity and began to broaden as the grinding time increased.

The short-range order of clays and the evolution of chemical groups with treatment were analyzed by the FTIR technique. Fig. 2 includes the FTIR spectra of the starting and ground montmorillonite clay samples. In the unmilled sample, the absorption bands at 3630 cm^{-1} and 3430 cm^{-1} correspond to the stretching modes of OH groups in the octahedral sheet and adsorbed water molecules, respectively. The former band is typical for dioctahedral smectites with a high content of aluminum (Madejová, 2003). The broad absorption band at 1040 cm^{-1} can be attributed to the Si—O stretching vibration in the tetrahedral sheet. The bands at 525 and 468 cm^{-1} correspond to Al–O–Si and Si–O–Si bending vibrations modes, respectively (Maleki and Karimi-Jashni, 2017). Also, absorption bands in the range of 950 to 800 cm^{-1} provide information about the composition of the octahedral sheet. The band situated at the mentioned range can be assigned to the presence of AlAlOH (916 cm^{-1}), AlFeOH (879 cm^{-1}), and AlMgOH (850 cm^{-1}) bending modes. FTIR measurements provide insights into the changes in the structural OH groups of montmorillonite. Disruption of these OH groups can be inferred even after a very short treatment time. The well-defined band at 3630 cm^{-1} became broader and decreased significantly during the first 30 min of grinding, indicating the breakdown of structural -OH groups and disruption of the octahedral sheet. At longer grinding times, this band disappeared completely. A similar behavior was observed in the OH bending modes bands between 850 cm^{-1} and 920 cm^{-1}.

The absorption bands at 916 and 879 cm^{-1}, assigned to AlAlOH and AlFeOH vibration modes respectively, gradually decreased and completely disappeared after 60 min of grinding. Likewise, the absorption band at 850 cm^{-1}, corresponding to AlMgOH bending vibration, decreased significantly after 30 min of grinding.

The band of 3430 cm^{-1} was still present and tended to broaden after grinding, which indicates the presence of absorbed water on the clay surface. A similar behavior was followed by the absorption bands at 525 and 468 cm^{-1}, which decreased significantly in intensity after intensive grinding, corresponding to the Al–O–Si and Si–O–Si bending vibrations, respectively. However, the band at 1040 cm^{-1}, attributed to the Si—O

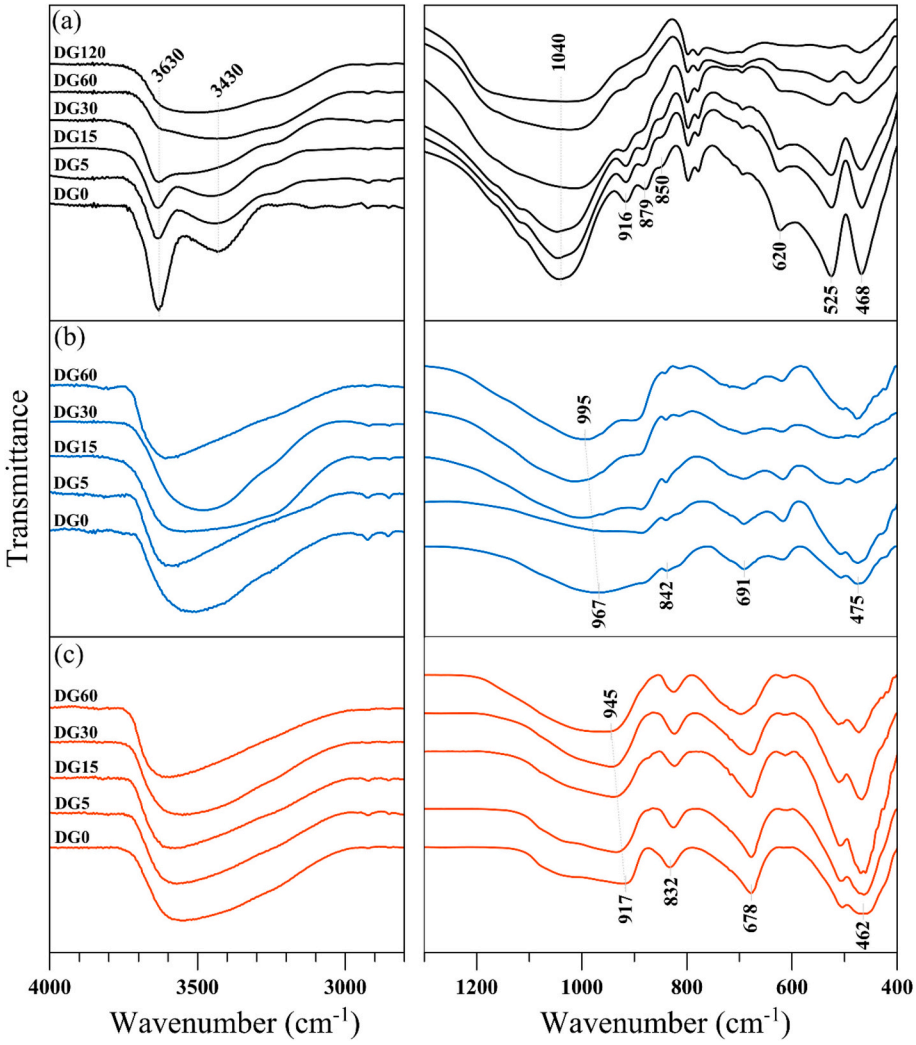

Fig. 2. IR spectra of the unmilled and ground (a) MMT, (b) Na-2-mica, and (c) Na-4-mica after different grinding times.

stretching vibration, exhibited an increased broadening during milling. These changes indicate the breakdown of the bonds between the tetrahedral and octahedral sheets in the montmorillonite samples, and consequently, the decomposition of the clay layers after 30 min of grinding.

Synthetic micas exhibited well-defined absorption bands due to their high-purity composition, obtained through the NaCl melt method (Fig. 2 (b) and (c)). The two well-resolved absorption bands at 3630 cm^{-1} and 3430 cm^{-1}, observed in the montmorillonite sample within the hydroxyl stretching region, appeared as a single envelope centered around ~3560 cm^{-1} in both synthetic micas. The absorption reflection at 3630 cm^{-1} was absent in synthetic micas, which was attributed to the substitution of structural OH groups with fluorine between the tetrahedral and octahedral sheets, due to the fluorinated nature of the reactants used in the synthesis process.

The portion of the spectra corresponding to lattice vibration was similar to that of fluorophlogopite, a synthetic mica with a similar composition, featuring a principal signal assigned to the [(Si,Al) —O] stretching mode at approximately 995 cm^{-1} (Gregorkiewitz and Rausell-Colom, 1987). The band wavenumber shifts to lower values as the aluminum content increases. The band at 832 cm^{-1} was assigned to the stretching of Al–O–Al bonds, while the bands at 690 cm^{-1} and 670 cm^{-1} correspond to Si—O stretching and bending vibrations, respectively (Farmer, 1958; Trujillano et al., 2010). Finally, the broad band centered at 487 cm^{-1} was assigned to the sum of the Si–O–Si bending, and Mg—O stretching modes (Yang et al., 2024). Grinding treatment in synthetic Na-2-mica and Na-4-mica caused fewer structural changes compared to natural clays. The absorption band at 3560 cm^{-1} in the micas was not significantly affected by the milling conditions, indicating the continued presence of water molecules on the clay. Similar behavior is observed in the fingerprint region, where the 1000 to 400 cm^{-1} spectral range provided valuable information on structural modifications within the mica layers. Ground Na-2-mica samples presented a slight decrease in intensity and broadening of the absorption bands at 690 cm^{-1} and 670 cm^{-1}, associated with the Si—O group in the tetrahedral sheet, indicating some impact of MCA in the mica layers up to 60 min of grinding. Consequently, a slight increase in the broadening of the Si—O band at 1000 cm^{-1} was also evident, which was indicative of the initial stages of amorphization in the tetrahedral sheets of Na-2-mica. Moreover, ground Na-4-mica samples performed even more structural stability than Na-2-micas. All characteristic absorption bands appeared to retain their intensity in the spectra of ground Na-4-mica, with only a slight broadening of the Si—O stretching band at 1000 cm^{-1}. The bands at 487 cm^{-1}, assigned to Mg—O stretching and Si–O–Si bending modes, remain almost unaffected in both micas. This finding aligns with earlier studies indicating that trioctahedral clays were generally more resistant to lattice distortion than their dioctahedral counterparts.

TG analysis was employed to monitor the hydration capacity of the clays and the evolution of OH groups throughout the grinding process. Fig. 3(a) includes the TG curves of the montmorillonite sample before

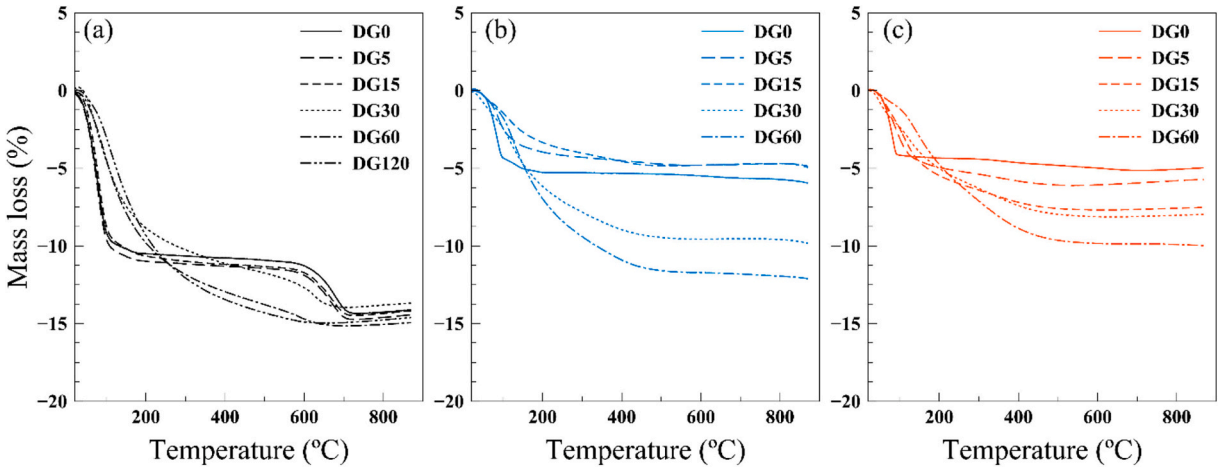

Fig. 3. Thermogravimetric curves of the unmilled and ground MMT (a), Na-2-mica (b), and Na-4-mica (c) samples after different grinding times.

and after grinding for progressively longer durations up to 120 min. In the case of the unmilled natural clay, the thermal analysis presented two main mass loss steps. The first step, occurring below 200 °C (10.5 %mass loss), corresponds to the release of weakly bound water molecules on the montmorillonite surface, as well as water from the clay interlayers. The second step began above 600 °C and it is associated with a 3.6 %mass loss, corresponding to the release of structural OH groups from the montmorillonite layers, indicating complete dehydroxylation of the clay sheets.

The TG curves of montmorillonite samples treated for up to 15 min were similar to those of the untreated material. This behavior was consistent with the XRD results, which presented no structural changes in the long-range order. However, as the grinding time increases beyond 15 min, notable modifications began to appear in the thermal behavior, suggesting the onset of structural alterations at the short-range level. After the mechanochemical treatment of montmorillonite, a significant change was observed in both the first and second main mass loss steps. Specifically, the second mass loss step (above 600 °C) began to decrease after 30 min of grinding, as dehydroxylation occurs at lower temperatures compared to the unmilled sample. This suggests that hydroxyl groups became more easily broken down with increasing temperature after treatment. The destruction of -OH bonds between the tetrahedral and octahedral sheets is consistent with the observations made in the FTIR spectra at that grinding time. After 60 min of milling, the TG curve of the sample consisted of a continuous mass loss, along with the disappearance of the characteristic plateau observed between 200 and 600 °C in clays. This behavior was consistent with the destruction of the layered structure and the amorphization of the material.

Fig. 3(b) and (c) include the TG curves of Na-*n*-micas before and after mechanical activation. Due to their fluorinated nature, both unmilled micas exhibited a single main mass loss step in the curve. This mass loss, occurring below 200 °C (5.3 %mass loss), corresponds to the release of adsorbed and interlayer water molecules in clay. Na-*n*-micas exhibited significantly greater structural stability compared to montmorillonite. As grinding time increased, a progressive modification of the thermogravimetric curve was followed, with the main mass loss step extending up to 400 °C. This result indicates that mechanical activation caused modifications in the clay's layered structure, primarily affecting the stacking arrangement of layers in synthetic micas. Beyond this temperature, the characteristic plateau of clay minerals was still maintained.

3.2. *Effect of dry grinding on clay textural properties*

Dry grinding causes effects on the structural layers through morphological modifications and particle size reduction in clays. Therefore, SEM and TEM techniques have been employed to characterize the particle morphology and size of the samples.

Fig. 4(a.1) and (a.2) present the MMT SEM images before and after dry milling. Owing to the intrinsic layered structure of clay minerals, the material tended to form relatively large agglomerates, often measuring approximately five microns or more in diameter, which can be readily detected through microscopy. Due to the large size of the agglomerates, the layers are not observable in the image. After 15 min of mechanical activation, fragmentation of the agglomerates can be observed, and after 30 min, the agglomerates became more spherical. TEM image (Fig. S1 of the unmilled montmorillonite allows to distinguish the clay-layered structure. The platelets exhibited a range of sizes, with a main particle size of 590 nm, making them polydisperse. After 15 min of treatment, the particles still displayed the characteristic pseudo-hexagonal shape of montmorillonite and appeared delaminated. After 30 min, a significant decrease in particle size became evident, with a particle size reduction of more than three times, resulting in a main particle size of 160 nm. This is followed by partial agglomeration of the hexagonal particles, leading to a rounded shape after 60 min of grinding.

Fig. 4 includes the SEM images of Na-2-mica and Na-4-mica. The SEM images of the raw samples revealed the laminar structure and stacked layers of both micas. After 15 min the morphological changes caused by the milling process can be observed in the images. The mechanical grinding process significantly affected the morphology of the particles, leading to a noticeable transformation in their shape. Initially characterized by well-defined, platy structures, the particles gradually lost their angular and layered features as grinding progresses. This resulted in a morphological shift toward more rounded and less structured forms.

The hexagonal structure of the synthetic clays was observable at the nanometric scale through TEM analysis (Figs. S2 and S3). The unmilled Na-2-mica and Na-4-mica exhibited mean particle sizes of 1390 nm and 1570 nm, respectively, and displayed a well-defined hexagonal morphology with a highly laminated structure. After mechanical activation, a gradual loss of the original layer shape was detected, particularly at the edges, up to 30 min of grinding. With extended grinding time (around 60 min), the particles evolved into rounded hexagonal shapes. Parallelly, a gradual reduction of particle size was also evident.

As mentioned above, mechanical activation of clay minerals led to significantly modifying the particle size distribution of montmorillonite and Na-n-micas, as illustrated in Fig. 5. The size distributions were calculated based on the analysis of at least 100 particles per sample. Due to their hexagonal shape, the particles were measured considering their longest diameter.

Before treatment, the three clays exhibited a high degree of polydispersity in particle size, as indicated by the wide range of sizes in the histograms. Montmorillonite had an average particle size of 593 nm,

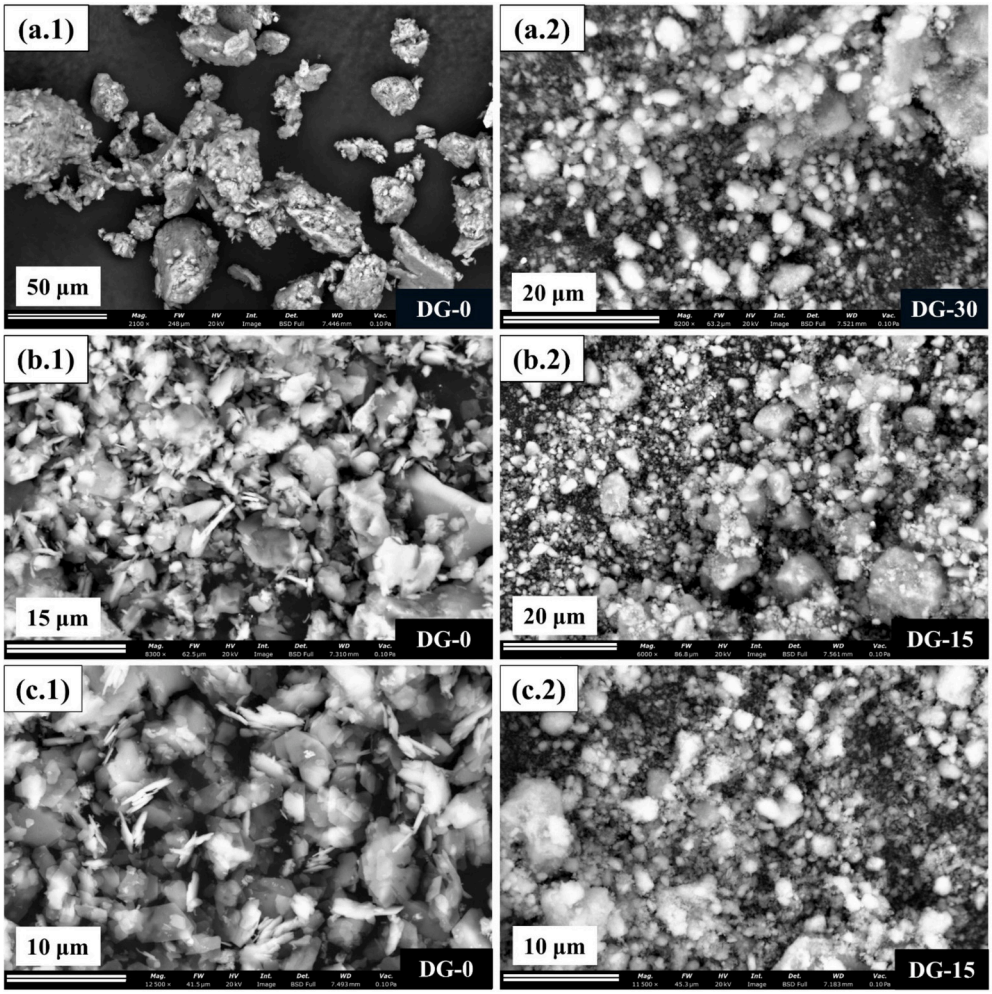

Fig. 4. SEM images of unmilled MMT (a.1) and ground MMT for 30 min (a.2) at the top. In the middle, SEM images of unmilled Na-2-mica (b.1) and ground Na-2-mica for 15 min (b.2). At the bottom, SEM images of unmilled Na-4-mica (c.1) and ground Na-4-mica for 15 min (c.2).

whereas Na-2-mica and Na-4-mica had at least two distinct particle size populations, with main sizes of approximately 1390 nm and 1570 nm, respectively. A progressive decrease in particle size was involved with increased grinding time (values are summarized in Table 1), reaching 70 nm for montmorillonite, 200 nm for Na-2-mica, and 370 nm for Na-4-mica, along with a reduction in polydispersity. However, prolonged grinding times led to an increase and stabilization of particle size due to the aggregation of nanoparticles. As grinding time increases, the reduction in particle size reached a steady state size under the given milling conditions, (Fig. 6). The different particle size value obtained comparing the three studied clays can be ascribed to competition between fracturing and crystal growth processes. Specifically, different material hardness and structural stability play a crucial role. Montmorillonite reached its minimum particle size after 60 min of grinding under these milling conditions, with a mean value of 70 nm. Meanwhile, Na-*n*-micas reached their minimum particle sizes of 200 nm and 370 nm after 30 min of grinding for $n = 2$ and $n = 4$, respectively. At the optimal grinding time (30 min), the particle size of montmorillonite was reduced by up to 73 % of its original size, while the particle sizes of Na-*n*-micas were reduced by up to 86 % and 77 % for $n = 2$ and 4, respectively. However, prolonged grinding of the montmorillonite sample also led to structural destruction and amorphization, as evidenced by the diffractogram, where after 60 min of grinding, only the quartz phase remained.

The evolution of the specific surface area and porosity with grinding was analyzed using nitrogen adsorption-desorption experiments. Fig. S4 includes the nitrogen adsorption-desorption isotherms of the samples before and after mechanical treatment, while the values of the total specific surface area (S_{BET}), specific surface area of micropores ($S_{\mu p}$), and external surface area (S_{ext}) are listed in Table 1. The isotherm of the montmorillonite sample before treatment was identified as Type II, which is characteristic of non-porous or macroporous materials, according to the literature (Sing et al., 1985). Although the montmorillonite sample exhibited both microporosity and mesoporosity, the total surface area was very low, 28 m^2/g, indicating that the contribution from microporosity was relatively low compared to classical microporous materials such as zeolites or pillared clays. Additionally, the mesoporosity is associated with the presence of a Type H3 hysteresis loop, which is related to capillary condensation of nitrogen in slit-shaped pores formed by aggregates of plate-like particles (Sing et al., 1985). Mechanical activation of montmorillonite led to a progressive increase in total surface area with grinding, which correlates with the decrease in particle size observed in the TEM images.

Samples ground for up to 30 min retained a similar Type II isotherm with a Type H3 hysteresis loop, and the specific surface area of micropores remained constant at approximately 17 m^2/g (Table 1). The isotherm of montmorillonite ground for longer durations exhibited a progressive decrease in the characteristic hysteresis loop associated with slit-like pores, eventually disappearing completely. This behavior indicates a significant alteration of the sample's morphology. Additionally, in the high relative pressure region, near $P/P_0 = 1$, the isotherms exhibited a rapid upward trend indicating the presence of macropores.

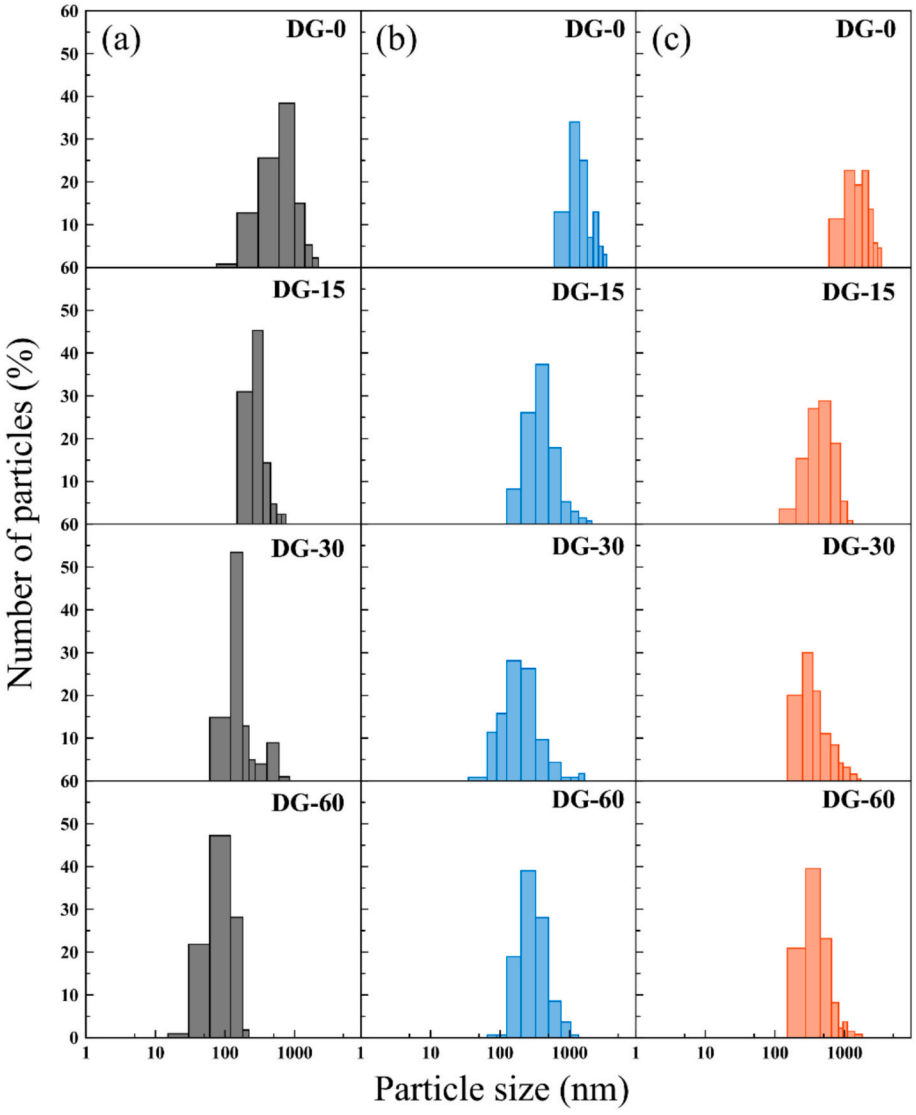

Fig. 5. Particle size distribution of unmilled and ground MMT (a), Na-2-mica (b) and Na-4-mica (c) after different grinding times.

Table 1
Mean particle size, specific surface area (S_{BET}), t-plot micropore area ($S_{\mu p}$), external surface area (S_{ext}), of MMT and Na-*n*-micas (n = 2,4) at different grinding times.

Clay	t (min)	Mean particle size (nm)	Textural properties		
			S_{BET} (m^2/g)	$S_{\mu p}$ (m^2/g)	S_{ext} (m^2/g)
MMT	0	590	28	11.6	16.2
	5	–	36	17.2	18.8
	15	260	38	17.5	20.3
	30	160	62	17.5	44.7
	60	70	83	13.0	70.1
	120	100	42	–	44.1
Na-2-mica	0	1390	7	4.5	2.9
	5	700	14	3.1	10.5
	15	370	9	1.0	8.4
	30	200	21	3.2	17.5
	60	260	20	1.6	18.7
Na-4-mica	0	1570	6	4.0	1.8
	5	810	28	2.7	25.3
	15	410	28	6.3	21.9
	30	370	17	0.9	16.1
	60	370	16	2.1	13.7

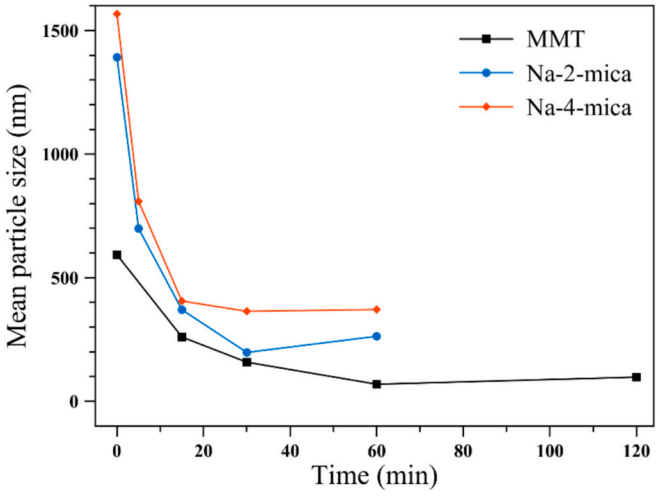

Fig. 6. Mean particle size of the unmilled and ground MMT, Na-2-mica, and Na-4-mica samples as a function of grinding time.

At 120 min the specific surface area decreased due to the tendency of the particles to aggregate.

The two synthetic micas presented a Type II isotherm, as defined by the International Union of Pure and Applied Chemistry (IUPAC) classification, typically linked to non-porous materials. The low BET surface area obtained for Na-2-mica, 7 m^2/g, and for Na-4-mica, 6 m^2/g, was consistent with this characterization. In contrast to montmorillonite, these samples did not exhibit mesoporosity related to the aggregate formation of platelet particles, as indicated by the absence of the hysteresis loop. The specific surface area increased progressively with grinding time, reaching a maximum at 30 min for Na-2-mica and at 15 min for Na-4-mica. Beyond these points, the surface area decreased, likely due to particle agglomeration. In parallel, particle size also decreases following a similar trend. Similar to montmorillonite ground for longer durations, the isotherms exhibit a sharp increase in the high relative-pressure range near $P/P_o = 1$, indicating the presence of macropores. Also, the surface area corresponding to the micropores remained low in both micas, attributing the increase in specific surface area to the external surface due to the reduction in particle size.

4. Conclusions

Dry grinding was employed here as a viable top-down nano-sintering technique to produce mechanically activated nano-clays from the high-charge mica group. Decreasing the particle size increases the number of exposed active sites, which is particularly important for the retention of high-level radioactive waste via the formation of new crystalline phases under hydrothermal conditions. In this mechanism, the active sites are associated with aluminum atoms located in the tetrahedral sheet of the aluminosilicate structure. Nanoscale reduction further enhances the exposure of aluminum ions on the surface, potentially leading to increased reactivity of the nanoclays. Extended treatment durations and gentle milling conditions were employed in a planetary ball mill to minimize amorphization or sample degradation as much as possible. A significant particle size reduction from microns to the nanoscale—approximately 74 %—was achieved after 15 min of grinding at 500 rpm, without modifying their long and short-range order. At these experimental conditions, mechanical activation led to alterations in the layered structure of the clay, with a notable impact on the stacking configuration of layers in synthetic micas. Nevertheless, the short-range structural order, characteristic chemical groups, and overall morphology of the micas remain preserved after the treatment. Even after extended grinding, an increase in external surface area is still evident, and the distinctive features of micas are retained in both X-ray diffraction patterns and infrared spectra. The trioctahedral nature of micas, along with their high aluminum content in the tetrahedral sheets, enhances their resistance to structural degradation. In contrast, montmorillonite—a dioctahedral smectite—completely lost its structure after 60 min of grinding. Finally, the reduction in particle size reached a steady state value under the specified milling conditions, which varies depending on the characteristics of each clay. Future research will focus on evaluating the capacity of the synthesized nanoclays to retain contaminant ions under ambient conditions, as a preliminary step toward their application in environmental remediation. Additionally, the reactivity of the nanoparticles to form new crystalline phases under hydrothermal conditions will be investigated and compared to that of the original high-charge mica. These studies will provide further insights into the advantages of particle size reduction, particularly regarding the enhancement of surface reactivity and structural transformation potential, with implications for their use in advanced applications such as radioactive waste confinement and critical element recovery.

CRediT authorship contribution statement

Aníbal López-Marín: Writing – original draft, Investigation, Formal analysis, Data curation. **Fernando Aguado:** Writing – review & editing, Writing – original draft, Supervision, Investigation, Funding acquisition, Conceptualization. **Rosa Martín-Rodríguez:** Writing – review & editing, Writing – original draft, Investigation, Funding acquisition, Conceptualization. **Ana C. Perdigón:** Writing – review & editing, Writing – original draft, Supervision, Investigation, Funding acquisition, Conceptualization.

Declaration of competing interest

The authors declare that they have no known competing financial interests or personal relationships that could have appeared to influence the work reported in this paper.

Acknowledgement

This project has received funds from MICIU/AEI/10.13039/501100011033 and the European Union-NextGenerationEU/PRTR TED2021-131305B-I00. López-Marín A. thanks to Cantabria Government's and University of Cantabria's fellowship "Concepción Arenal" for predoctoral formation.

Appendix A. Supplementary data

Supplementary data to this article can be found online at https://doi.org/10.1016/j.clay.2025.107969.

Data availability

Data will be made available on request.

References

Alba, M.D., Castro, M.A., Naranjo, M., Pavón, E., 2006. Hydrothermal reactivity of Na-n-micas (n = 2, 3, 4). Chem. Mater. 18, 2867–2872. https://doi.org/10.1021/cm0514802.

Alshameri, A., He, H., Xin, C., Zhu, J., Xinghu, W., Zhu, R., Wang, H., 2019. Understanding the role of natural clay minerals as effective adsorbents and alternative source of rare earth elements: Adsorption operative parameters. Hydrometallurgy 185, 149–161. https://doi.org/10.1016/j.hydromet.2019.02.016.

Baláž, P., Achimovicová, M., Baláž, M., Billik, P., Zara, C.Z., Criado, J.M., Delogu, F., Dutková, E., Gaffet, E., Gotor, F.J., Kumar, R., Mitov, I., Rojac, T., Senna, M., Streletskii, A., Krystyna, W.C., 2013. Hallmarks of mechanochemistry: from nanoparticles to technology. Chem. Soc. Rev. 42, 7571–7637. https://doi.org/10.1039/c3cs35468g.

Bekri-Abbes, I., Srasra, E., 2016. Effect of mechanochemical treatment on structure and electrical properties of montmorillonite. J. Alloys Compd. 671, 34–42. https://doi.org/10.1016/j.jallcom.2016.02.048.

Christidis, G.E., Dellisanti, F., Valdre, G., Makri, P., 2005. Structural modifications of smectites mechanically deformed under controlled conditions. Clay Miner. 40, 511–522. https://doi.org/10.1180/0009855054040188.

Dellisanti, F., Minguzzi, V., Valdrè, G., 2011. Mechanical and thermal properties of a nanopowder talc compound produced by controlled ball milling. J. Nanopart. Res. 13, 5919–5926. https://doi.org/10.1007/s11051-011-0541-6.

Elhadj, M.S.Y., Perrin, F.X., 2021. Influencing parameters of mechanochemical intercalation of kaolinite with urea. Appl. Clay Sci. 213. https://doi.org/10.1016/j.clay.2021.106250.

Fang, Z., Suhua, H., Xu, L., Jian, F., Qi, L., Zhiwei, W., Chuanchang, L., Yuanlai, X., 2021. Adsorption kinetics and thermodynamics of rare earth on Montmorillonite modified by sulfuric acid. Colloids Surf. A Physicochem. Eng. Asp. 627. https://doi.org/10.1016/j.colsurfa.2021.127063.

Farmer, V.C., 1958. The infra-red spectra of talc, saponite, and hectorite. Mineral. Mag. J. Mineral. Soc. 31, 829–845. https://doi.org/10.1180/minmag.1958.031.241.03.

Frost, R.L., Makó, É., Kristóf, J., Horváth, E., Kloprogge, J.T., 2001. Modification of kaolinite surfaces by mechanochemical treatment. Langmuir 17, 4731–4738. https://doi.org/10.1021/la001453k.

Gregorkiewitz, M., Rausell-Colom, J.A., 1987. Characterization and properties of a new synthetic silicate with highly charged mica-type layers. Am. Mineral. 72, 515–527.

Hrachová, J., Komadel, P., Fajnor, V.Š., 2007. The effect of mechanical treatment on the structure of montmorillonite. Mater. Lett. 61, 3361–3365. https://doi.org/10.1016/j.matlet.2006.11.063.

Iannicelli-Zubiani, E.M., Cristiani, C., Dotelli, G., Gallo Stampino, P., Pelosato, R., Mesto, E., Schingaro, E., Lacalamita, M., 2015. Use of natural clays as sorbent materials for rare earth ions: Materials characterization and set up of the operative parameters. Waste Manag. 46, 546–556. https://doi.org/10.1016/j.wasman.2015.09.017.

Ji, B., Zhang, W., 2021. The effect of mechanical grinding and thermal treatment on the recovery of rare earth elements (REEs) from kaolinite. Powder Technol. 394, 622–631. https://doi.org/10.1016/j.powtec.2021.08.077.

Kim, H.N., Kim, J.W., Kim, M.S., Lee, B.H., Kim, J.C., 2019. Effects of ball size on the grinding behavior of talc using a high-energy ball mill. Minerals 9. https://doi.org/10.3390/min9110668.

Kim, J., Hong, S., Lee, G., Um, W., 2025. Functionalization of layered double hydroxides on bentonite for cesium and iodine retention in high-level radioactive waste disposal. Chemosphere 370, 144014. https://doi.org/10.1016/j.chemosphere.2024.144014.

Machida, S., Katsumata, K., Yasumori, A., 2023. Effect of particle size of calcite on the stacking order of kaolinite during mechanical grinding. Int. J. Ceramic Eng. Sci. 5. https://doi.org/10.1002/ces2.10165.

Madejová, J., 2003. FTIR techniques in clay mineral studies. Vib. Spectrosc. 31, 1–10. https://doi.org/10.1016/S0924-2031(02)00065-6.

Maleki, S., Karimi-Jashni, A., 2017. Effect of ball milling process on the structure of local clay and its adsorption performance for Ni(II) removal. Appl. Clay Sci. 137, 213–224. https://doi.org/10.1016/j.clay.2016.12.008.

Mañosa J. la de Rosa J.C. Silvello A. Maldonado-Alameda A. Chimenos J.M. 2023 Kaolinite structural modifications induced by mechanical activation Appl. Clay Sci. 238 https://doi.org/10.1016/j.clay.2023.106918.

Morantes, C.F., Yarza, F., Montes, M.L., Mercader, R.C., Curutchet, G., Torres Sánchez, R. M., 2020. Sorbent Materials Characterization based on Mechanical or thermal Pretreated Montmorillonite Modified by Surfactant Loading for improved Chromium Retention. Water Air Soil Pollut. 231. https://doi.org/10.1007/s11270-020-4403-7.

Nasser, A., Mingelgrin, U., 2012. Mechanochemistry: a review of surface reactions and environmental applications. Appl. Clay Sci. 67–68, 141–150. https://doi.org/10.1016/j.clay.2011.11.018.

Osuna, F.J., Fernández, M., Pavón, E., Torres Sánchez, R.M., Alba, M.D., 2023. Mechanical treatments on design powder ceramic materials: Insight into the textural and structural changes. Adv. Powder Technol. 34. https://doi.org/10.1016/j.apt.2023.104189.

Pálková, H., Barlog, M., Madejová, J., Hronský, V., Petra, L., Šimon, E., Billik, P., Zimowska, M., 2021. Structural changes in smectites subjected to mechanochemical activation: the effect of the occupancy of the octahedral sites. Appl. Clay Sci. 213. https://doi.org/10.1016/j.clay.2021.106214.

Said, A., Zhang, Q., Qu, J., Liu, Y., Lei, Z., Hu, H., Xu, Z., 2018. Mechanochemical activation of phlogopite to directly produce slow-release potassium fertilizer. Appl. Clay Sci. 165, 77–81. https://doi.org/10.1016/j.clay.2018.08.006.

Sanchez-Soto, P.J., Perez-Rodriguez, J.L., 1989. Formation of Mullite from Pyrophyllite by Mechanical and thermal Treatments. J. Am. Ceram. Soc. 72, 154–157. https://doi.org/10.1111/j.1151-2916.1989.tb05972.x.

Sing, K.S.W., Everett, D.H., Haul, R.A.W., Moscou, L., Pierotti, R.A., Rouquerol, J., Siemieniewska, T., 1985. Reporting Physisorption Data for Gas/Solid Systems with special Reference to the Determination of Surface Area and Porosity. Pure Appl. Chem. 57, 603–619. https://doi.org/10.1351/pac198557040603.

Tole, I., Habermehl-Cwirzen, K., Cwirzen, A., 2019. Mechanochemical activation of natural clay minerals: an alternative to produce sustainable cementitious binders – review. Mineral. Petrol. 113, 449–462. https://doi.org/10.1007/s00710-019-00666-y.

Trujillano, R., Rico, E., Vicente, M.A., Herrero, M., Rives, V., 2010. Microwave radiation and mechanical grinding as new ways for preparation of saponite-like materials. Appl. Clay Sci. 48, 32–38. https://doi.org/10.1016/j.clay.2009.11.018.

Valera-Zaragoza, M., Agüero-Valdez, D., Lopez-Medina, M., Dehesa-Blas, S., Karin Navarro-Mtz, A., Avalos-Borja, M., Juarez-Arellano, E.A., 2021. Controlled modification of sodium montmorillonite clay by a planetary ball-mill as a versatile tool to tune its properties. Adv. Powder Technol. 32, 591–599. https://doi.org/10.1016/j.apt.2021.01.004.

Vdovic, N., Jurina, I., Škapin, S.D., Sondi, I., 2010. The surface properties of clay minerals modified by intensive dry milling - revisited. Appl. Clay Sci. 48, 575–580. https://doi.org/10.1016/j.clay.2010.03.006.

Xia, M., Jiang, Y., Zhao, L., Li, F., Xue, B., Sun, M., Liu, D., Zhang, X., 2010. Wet grinding of montmorillonite and its effect on the properties of mesoporous montmorillonite. Colloids Surf. A Physicochem. Eng. Asp. https://doi.org/10.1016/j.colsurfa.2009.12.014.

Xiao, Y., Huang, L., Long, Z., Feng, Z., Wang, L., 2016. Adsorption ability of rare earth elements on clay minerals and its practical performance. J. Rare Earths 34, 543–548. https://doi.org/10.1016/S1002-0721(16)60060-1.

Yang, Z., He, M., Wu, S., Yang, M., Peng, B., 2024. Near-infrared spectroscopic study of biotite–phlogopite (Mg# = 30~99): OH-stretching modes and Mg# content prediction equation. Crystals 14. https://doi.org/10.3390/cryst14040336.

Zhang, J., Yan, J., Sheng, J., 2015. Dry grinding effect on pyrophyllite-quartz natural mixture and its influence on the structural alternation of pyrophyllite. Micron 71, 1–6. https://doi.org/10.1016/j.micron.2014.12.005.